Elasto-plasticity model in structural optimization of composite materials with periodic microstructures

Ronald H.W. Hoppe[a,b], Svetozara I. Petrova[a,c,*]

[a] *Institute of Mathematics, University of Augsburg, D-86159 Augsburg, Germany*
[b] *Department of Mathematics, University of Houston, Houston, TX 77204-3008, USA*
[c] *Institute for Parallel Processing, Bulgarian Academy of Sciences, 1113 Sofia, Bulgaria*

1. Introduction

Structural optimization of biomorphic cellular ceramics with specific microstructures is considered. The new composite materials are designed and produced by biotemplating processing using a naturally grown wood which is known to be highly porous and to possess excellent mechanical properties. High temperature pyrolysis of the wooden specimen followed by an infiltration of liquid- or gaseous-phase metals such as silicon (Si) or titanium (Ti) come up to silicon carbide (SiC)- or titanium carbide (TiC)-ceramics of high porosity. The biomimetic processing scheme for production of SiC-ceramics from wood is explained in [15]. The new ceramic composites can be used as filters in chemical processing, as implant material in biomedical applications or as high performance brakes of vehicles in car industry.

The optimization of the macroscopic behavior of microstructural materials using microscopic quantities as design variables is a well established discipline in materials science (cf., [1,6,12]). Homogenization techniques are applied to

* Corresponding author. Tel.: +49 821 5982312; fax:+49 821 5982339.
E-mail address: petrova@math.uni-augsburg.de (S.I. Petrova).

come up with computationally feasible macromodels. The microstructural geometrical details of the microcells such as the lengths and widths of the different layers forming the cell walls are considered as design parameters which have a significant impact on the macroscopic mechanical behavior of the final ceramics. Moreover, they can be tuned very precisely during the processing procedures. Therefore, the idea is to determine these details in order to achieve an optimal operational behavior with respect to selected mechanical merit functionals under prespecified load conditions.

Recently, we have developed algorithmic tools for the computation of the homogenized model (homogenized elasticity tensor) and its dependence on the design variables as well as efficient and reliable structural optimization routines based on an "all-at-once" approach that is superior to traditional techniques (see, [9,10]). Mesh adaptivity schemes for the numerical solution of the elasticity problem defined in a three-dimensional microcell and appropriate iterative methods for the discretized state equation in the homogenized macromodel are considered and discussed in [11].

In this paper, we formulate the problem for structural optimization of the composite ceramic materials invoking an elasto-plasticity in the macroscopic model by using the von Mises yield criterion with isotropic strain hardening. Section 2 contains the general elasto-plastic constitutive relations under the assumption of small strains. An incremental finite element algorithm is presented in Section 3 for the numerical solution of the elasto-plastic problem. Return mapping procedures, first developed in [21] for simple plasticity models, based on the concept of computing a trial elastic stress (elastic stress predictor) mapped onto a suitably updated yield surface (plastic return corrector) are applied in Section 4 to find the new stress during the time increment. In the last years, the latter methods became rather popular tools to provide efficient and accurate computations for constitutive modeling (see, e.g., [17,2,5,19,22]). The problem of optimal structural design of biomorphic TiC-ceramics (ductile materials) is discussed in Section 5. The macroscopic model is based on the homogenization approach to compute the constitutive expressions. The homogenized elasto-plastic equation is considered as an equality constraint in the structural optimization problem. Adaptive grid refinement in space based on a posteriori error estimators is applied at each time step within the incremental finite element method. Numerical experiments for the computation of the homogenized elasticity coefficients using a three-dimensional periodicity microcell are presented. Applications of Newton-like iterative solvers for the nonlinear systems arising in the numerical solution of the elasto-plastic problem are commented. Some concluding remarks are given in the last section.

The following standard notations are used throughout this paper. Bold-face symbols indicate variables of tensorial character. By the convention of a summation on repeated indices, dots are used for a scalar product of vectors, e.g., $\boldsymbol{u} \cdot \boldsymbol{v} = u_i v_i$ and colons (:) are used for a scalar product of tensors, e.g., $(\boldsymbol{E} : \boldsymbol{e})_{ij} = E_{ijkl} e_{kl}$, $(\boldsymbol{A} : \boldsymbol{B}) = A_{ij} B_{ij}$. The norm of a second-order tensor is denoted by $\|\boldsymbol{S}\| = (\boldsymbol{S} : \boldsymbol{S})^{1/2} = (S_{ij} S_{ij})^{1/2}$. The symbol $\otimes$ indicates the tensor product of vectors and tensors defined by $(\boldsymbol{u} \otimes \boldsymbol{v})_{ij} = u_i v_j$ and $(\boldsymbol{A} \otimes \boldsymbol{B})_{ijkl} = A_{ij} B_{kl}$.

2. Elasto-plasticity

Let us consider an elasto-plastic material body occupying a bounded Lipschitz domain $\Omega \subset \mathcal{R}^3$. For describing the development of plastic strains, we introduce a time/load (continuation) parameter t, $0 \le t \le T$ and find the deformations of the body following the history of loading. The dot below denotes the derivative with respect to the parameter t.

Given a displacement field $\boldsymbol{u} = \boldsymbol{u}(t) \in [H^1(\Omega)]^3$, the total small strain reads

$$\boldsymbol{e} = \frac{\nabla \boldsymbol{u} + (\nabla \boldsymbol{u})^{\mathrm{T}}}{2}, \quad \text{i.e., } e(\boldsymbol{u})_{ij} = \frac{u_{i,j} + u_{j,i}}{2};\ 1 \le i, j \le 3. \tag{1}$$

The following governing equations describe the elasto-plastic behavior of the material

$$\boldsymbol{e} = \boldsymbol{e}^{\mathrm{e}} + \boldsymbol{e}^{\mathrm{p}} \tag{2}$$

$$\dot{\boldsymbol{e}} = \dot{\boldsymbol{e}}^{\mathrm{e}} + \dot{\boldsymbol{e}}^{\mathrm{p}} \tag{3}$$

$$\boldsymbol{\sigma} = \boldsymbol{E} : \boldsymbol{e}^{\mathrm{e}} \tag{4}$$

$$\Phi(\boldsymbol{\sigma}, \boldsymbol{\xi}) = 0 \tag{5}$$

$$\dot{\boldsymbol{e}}^{\mathrm{p}} = \gamma \frac{\partial G}{\partial \boldsymbol{\sigma}} \tag{6}$$

$$\dot{\boldsymbol{\xi}} = \gamma z, \tag{7}$$

where the total strain $\boldsymbol{e}$ is decomposed into an elastic and plastic strain tensors denoted by $\boldsymbol{e}^{\mathrm{e}}$ and $\boldsymbol{e}^{\mathrm{p}}$, respectively, $\boldsymbol{\sigma}$ the Cauchy stress tensor, $\boldsymbol{E}$ the fourth-order elasticity tensor, $\Phi = \Phi(\boldsymbol{\sigma}, \boldsymbol{\xi}) \leq 0$ the yield function, $\boldsymbol{\xi} \in \mathcal{R}^k$, $k \geq 1$, the vector of internal state variables, $\gamma \geq 0$ the plastic multiplier (also called the magnitude of the plastic strain rate), G the flow potential, and $\boldsymbol{z}$ is a vector related to the evolution of the internal state variables $\boldsymbol{\xi}$. Note that $\boldsymbol{\xi}$ and $\boldsymbol{z}$ are scalars in the case $k = 1$. We assume that the scalar-valued function G is differentiable everywhere and $\partial G/\partial \boldsymbol{\sigma}$ is a second-order tensor produced by differentiation of G with respect to the tensorial argument $\boldsymbol{\sigma}$.

Linear isotropic and homogeneous elasticity is considered, so that (4) is referred to Hooke's law which corresponds to a two-parameter model with nonzero material coefficients given as follows

$$E_{iiii} = \lambda + 2\mu, \qquad E_{iijj} = \lambda, \qquad E_{ijij} = E_{ijji} = 2\mu, \tag{8}$$

where $1 \leq i, j \leq 3$, $i \neq j$, and λ, μ are the Lamé moduli of the material. Very often in the literature the isotropic materials are also described by the Young modulus E and the Poisson ratio ν.

Eq. (5) defines the yield surface and can be viewed as the onset of the inelastic behavior of the material. The yield function Φ obeys the sign convention: elastic deformations correspond to negative values of Φ (the interior of the yield surface) and forbidden deformations (on the exterior of the yield surface) are identified by positive values of Φ. Hence, all admissible stresses are described by $\Phi(\boldsymbol{\sigma}, \boldsymbol{\xi}) \leq 0$ and exactly one of the following relations holds

$$\begin{aligned} &\gamma = 0 \wedge \Phi(\boldsymbol{\sigma}, \boldsymbol{\xi}) < 0, && \textit{elastic} \text{ behavior} \\ &\gamma > 0 \wedge \Phi(\boldsymbol{\sigma}, \boldsymbol{\xi}) = 0 \wedge \dot{\Phi}(\boldsymbol{\sigma}, \boldsymbol{\xi}) = 0, && \textit{plastic} \text{ behavior} \end{aligned} \tag{9}$$

These relations are explicitly described by the Karush–Kuhn–Tucker (KKT) loading/unloading conditions which take place both for elastic and plastic deformations

$$\gamma \geq 0, \quad \Phi(\boldsymbol{\sigma}, \boldsymbol{\xi}) \leq 0, \quad \gamma\Phi(\boldsymbol{\sigma}, \boldsymbol{\xi}) = 0. \tag{10}$$

The parameter $\gamma \geq 0$ in (10) is determined by the plastic consistency condition $\gamma\dot{\Phi}(\boldsymbol{\sigma}, \boldsymbol{\xi}) = 0$. Note that γ is nonzero only if $\Phi = \dot{\Phi} = 0$, see (9). For details we refer to [17].

The plastic flow rule is expressed by (6). In the case of associative plasticity (typically applied to porous solids) the flow function becomes $G = \Phi$ and the associative flow rule of plastic deformation is given by

$$\dot{\boldsymbol{e}}^{\mathrm{p}} = \gamma \frac{\partial \Phi}{\partial \boldsymbol{\sigma}}. \tag{11}$$

For rate-independent elasto-plasticity the relation (4) involves the rate constitutive equation $\dot{\boldsymbol{\sigma}} = \boldsymbol{E} : \dot{\boldsymbol{e}}^{\mathrm{e}}$. Using (3) and (11) the following expression holds

$$\dot{\boldsymbol{\sigma}} = \boldsymbol{E} : \left(\dot{\boldsymbol{e}} - \gamma \frac{\partial \Phi}{\partial \boldsymbol{\sigma}} \right). \tag{12}$$

Multiplying (12) by $\partial\Phi/\partial\boldsymbol{\sigma}$ we get

$$\frac{\partial \Phi}{\partial \boldsymbol{\sigma}} : \dot{\boldsymbol{\sigma}} = \frac{\partial \Phi}{\partial \boldsymbol{\sigma}} : \boldsymbol{E} : \dot{\boldsymbol{e}} - \gamma \frac{\partial \Phi}{\partial \boldsymbol{\sigma}} : \boldsymbol{E} : \frac{\partial \Phi}{\partial \boldsymbol{\sigma}}. \tag{13}$$

To eliminate γ we take the rate form of (5) as follows

$$\dot{\Phi}(\boldsymbol{\sigma}, \boldsymbol{\xi}) = 0, \tag{14}$$

which using the chain rule reads

$$\frac{\partial \Phi}{\partial \boldsymbol{\sigma}} : \dot{\boldsymbol{\sigma}} + \frac{\partial \Phi}{\partial \boldsymbol{\xi}} \cdot \dot{\boldsymbol{\xi}} = 0. \tag{15}$$

Replacing (13) and (7) in (15) we get the following expression

$$\frac{\partial \Phi}{\partial \boldsymbol{\sigma}} : \boldsymbol{E} : \dot{\boldsymbol{e}} - \gamma \left(\frac{\partial \Phi}{\partial \boldsymbol{\sigma}} : \boldsymbol{E} : \frac{\partial \Phi}{\partial \boldsymbol{\sigma}} - \frac{\partial \Phi}{\partial \boldsymbol{\xi}} \cdot \boldsymbol{z} \right) = 0. \tag{16}$$

Thus, the plastic multiplier can be defined explicitly as

$$\gamma = \frac{(\partial \Phi/\partial \boldsymbol{\sigma}) : \boldsymbol{E} : \dot{\boldsymbol{e}}}{(\partial \Phi/\partial \boldsymbol{\sigma}) : \boldsymbol{E} : (\partial \Phi/\partial \boldsymbol{\sigma}) - (\partial \Phi/\partial \boldsymbol{\xi}) \cdot z}. \tag{17}$$

Substituting γ in (12) we get

$$\dot{\boldsymbol{\sigma}} = \boldsymbol{E}^{\mathrm{ep}} : \dot{\boldsymbol{e}}, \tag{18}$$

where the so-called continuum elasto-plastic tangent modulus $\boldsymbol{E}^{\mathrm{ep}}$ is given by

$$\boldsymbol{E}^{\mathrm{ep}} = \boldsymbol{E}^{\mathrm{ep}}(\boldsymbol{\sigma}, \boldsymbol{\xi}, \dot{\boldsymbol{e}}) = \begin{cases} \boldsymbol{E}, & \text{if } \Phi(\boldsymbol{\sigma}, \boldsymbol{\xi}) < 0 \wedge \dfrac{\partial \Phi}{\partial \boldsymbol{\sigma}} : \boldsymbol{E} : \dot{\boldsymbol{e}} \le 0, \\ \boldsymbol{E} - \dfrac{\boldsymbol{E} : (\partial \Phi/\partial \boldsymbol{\sigma}) \otimes (\partial \Phi/\partial \boldsymbol{\sigma}) : \boldsymbol{E}}{(\partial \Phi/\partial \boldsymbol{\sigma}) : \boldsymbol{E} : (\partial \Phi/\partial \boldsymbol{\sigma}) - (\partial \Phi/\partial \boldsymbol{\xi}) \cdot z}, & \text{if } \Phi(\boldsymbol{\sigma}, \boldsymbol{\xi}) = 0 \wedge \dfrac{\partial \Phi}{\partial \boldsymbol{\sigma}} : \boldsymbol{E} : \dot{\boldsymbol{e}} > 0. \end{cases} \tag{19}$$

Using (17) one can rewrite (7) in the form

$$\dot{\boldsymbol{\xi}} = \boldsymbol{G}^{\mathrm{ep}} : \dot{\boldsymbol{e}}, \tag{20}$$

where

$$\boldsymbol{G}^{\mathrm{ep}} = \boldsymbol{G}^{\mathrm{ep}}(\boldsymbol{\sigma}, \boldsymbol{\xi}, \dot{\boldsymbol{e}}) = \begin{cases} \boldsymbol{0}, & \text{if } \Phi(\boldsymbol{\sigma}, \boldsymbol{\xi}) < 0 \wedge \dfrac{\partial \Phi}{\partial \boldsymbol{\sigma}} : \boldsymbol{E} : \dot{\boldsymbol{e}} \le 0, \\ \dfrac{(\partial \Phi/\partial \boldsymbol{\sigma}) : \boldsymbol{E} : z}{(\partial \Phi/\partial \boldsymbol{\sigma}) : \boldsymbol{E} : (\partial \Phi/\partial \boldsymbol{\sigma}) - (\partial \Phi/\boldsymbol{\xi}) \cdot z}, & \text{if } \Phi(\boldsymbol{\sigma}, \boldsymbol{\xi}) = 0 \wedge \dfrac{\partial \Phi}{\partial \boldsymbol{\sigma}} : \boldsymbol{E} : \dot{\boldsymbol{e}} > 0. \end{cases} \tag{21}$$

The expressions (18)and (20) are called the incremental elasto-plastic constitutive relations derived under the assumption (14) during the plastic yielding.

We suppose now that the elasto-plastic body occupying the domain Ω is fixed on the part Γ_{D} of its boundary $\partial\Omega$, $\Gamma_{\mathrm{D}} \subset \partial\Omega$, and loaded by the body force $\boldsymbol{f}_{\mathrm{b}}$ in Ω and by the surface traction $\boldsymbol{f}_{\mathrm{s}}$ on the rest part of the boundary Γ_T, $\Gamma_T \subset \partial\Omega$, $\Gamma_{\mathrm{D}} \cup \Gamma_T = \partial\Omega$. Taking into account the continuation of loading with respect to the time parameter $t \in [0, T] \subset \mathcal{R}$ one can formulate the problem of elasto-plasticity as the following initial value problem: find

$$\boldsymbol{u} = \boldsymbol{u}(\boldsymbol{x}, t), \qquad \boldsymbol{\sigma} = \boldsymbol{\sigma}(\boldsymbol{x}, t), \qquad \boldsymbol{\xi} = \boldsymbol{\xi}(\boldsymbol{x}, t),$$

such that

$$\begin{aligned} &\textstyle\int_{\Omega} \dot{\boldsymbol{\sigma}} : \boldsymbol{e}(\boldsymbol{v}) \,\mathrm{d}\Omega = (\dot{\boldsymbol{F}}, \boldsymbol{v}), \quad \forall \boldsymbol{v} \in \boldsymbol{V},\ t \in (0, T] \\ &\dot{\boldsymbol{\sigma}} = \boldsymbol{E}^{\mathrm{ep}}(\boldsymbol{\sigma}, \boldsymbol{\xi}, \dot{\boldsymbol{e}}) : \dot{\boldsymbol{e}} \\ &\dot{\boldsymbol{\xi}} = \boldsymbol{G}^{\mathrm{ep}}(\boldsymbol{\sigma}, \boldsymbol{\xi}, \dot{\boldsymbol{e}}) : \dot{\boldsymbol{e}} \\ &\dot{\boldsymbol{e}} = \boldsymbol{e}(\dot{\boldsymbol{u}}), \quad \dot{\boldsymbol{u}} \in \boldsymbol{V} \end{aligned} \tag{22}$$

with initial conditions

$$\boldsymbol{u} = \boldsymbol{u}(\boldsymbol{x}, 0) = \boldsymbol{0}, \qquad \boldsymbol{\sigma} = \boldsymbol{\sigma}(\boldsymbol{x}, 0) = \boldsymbol{0}, \qquad \boldsymbol{\xi} = \boldsymbol{\xi}(\boldsymbol{x}, 0) = \boldsymbol{0}, \quad \forall \boldsymbol{x} \in \Omega.$$

Here, $\boldsymbol{x}$ is the space variable in Ω, $\boldsymbol{V} := \{\boldsymbol{v} \in [H^1(\Omega)]^3 | \boldsymbol{v} = \boldsymbol{0} \text{ on } \Gamma_{\mathrm{D}}\}$ is the space of admissible displacements, and $\boldsymbol{F}$ is the function of all external forces with an inner product defined as follows

$$(\dot{\boldsymbol{F}}, \boldsymbol{v}) = \int_{\Omega} \dot{\boldsymbol{f}}_{\mathrm{b}} \cdot \boldsymbol{v} \,\mathrm{d}\Omega + \int_{\Gamma_T} \dot{\boldsymbol{f}}_{\mathrm{s}} \cdot \boldsymbol{v} \,\mathrm{d}\Gamma.$$

Note that the first relation in (22) represents the incremental equilibrium equation in a weak form.

3. Incremental finite element elasto-plasticity

In this section, we present the discrete analog of the initial value problem (22) by using finite differences with respect to the time parameter t and finite elements with respect to the space variable $\boldsymbol{x}$. We introduce the following

temporal mesh in the interval $[0, T] \subset \mathcal{R}$

$$t^0 = 0, \qquad t^{n+1} = t^n + \triangle t, \quad n = 0, \ldots, N, \; N = \frac{T}{\triangle t} - 1. \tag{23}$$

The domain Ω is discretized by finite elements with a discretization parameter h. Using rates one can exploit the following incremental relation

$$\triangle \boldsymbol{\sigma}_h = \int_{t^n}^{t^{n+1}} \dot{\boldsymbol{\sigma}}_h \, \mathrm{d}t, \quad t \in [t^n, t^{n+1}].$$

For a fixed time step $t^n = n \triangle t$ we approximate $\boldsymbol{u}(\boldsymbol{x}, t^n)$, $\boldsymbol{\sigma}(\boldsymbol{x}, t^n)$, and $\boldsymbol{\xi}(\boldsymbol{x}, t^n)$, respectively, by

$$\boldsymbol{u}_h^n(\boldsymbol{x}), \quad \boldsymbol{\sigma}_h^n(\boldsymbol{x}), \quad \boldsymbol{\xi}_h^n(\boldsymbol{x}),$$

where $\boldsymbol{u}_h^n \in \boldsymbol{V}_h$, $\boldsymbol{V}_h$ is the finite element subspace of $\boldsymbol{V}$, $\boldsymbol{\sigma}_h^n$ and $\boldsymbol{\xi}_h^n$ belong to the corresponding discrete spaces of stresses and internal variables.

For given $\boldsymbol{u}_h^n, \boldsymbol{\sigma}_h^n, \boldsymbol{\xi}_h^n$, the increments $\triangle \boldsymbol{u}_h$, $\triangle \boldsymbol{\sigma}_h$, $\triangle \boldsymbol{\xi}_h$ at the time step t^n, $n = 0, \ldots, N$, can be determined by using the following incremental finite element (FE) algorithm

S1. *Initial step*: $\boldsymbol{u}_h^0 = \boldsymbol{0}$, $\boldsymbol{\sigma}_h^0 = \boldsymbol{0}$, $\boldsymbol{\xi}_h^0 = \boldsymbol{0}$

S2. *Time steps*: **for** $n = 0, \ldots, N$ **do**

- Compute the increments $\triangle \boldsymbol{u}_h$, $\triangle \boldsymbol{\sigma}_h$, $\triangle \boldsymbol{\xi}_h$, such that

$$\int_\Omega \triangle \boldsymbol{\sigma}_h : \boldsymbol{e}(\boldsymbol{v}_h) \, \mathrm{d}\Omega = (\triangle \boldsymbol{F}, \boldsymbol{v}_h), \quad \forall \boldsymbol{v}_h \in \boldsymbol{V}_h, \tag{24}$$

$$\triangle \boldsymbol{\sigma}_h = \boldsymbol{E}^{\mathrm{ep}}(\boldsymbol{\sigma}_h^n + \theta \triangle \boldsymbol{\sigma}_h, \boldsymbol{\xi}_h^n + \theta \triangle \boldsymbol{\xi}_h, \triangle \boldsymbol{e}_h) : \triangle \boldsymbol{e}_h, \tag{25}$$

$$\triangle \boldsymbol{\xi}_h = \boldsymbol{G}^{\mathrm{ep}}(\boldsymbol{\sigma}_h^n + \theta \triangle \boldsymbol{\sigma}_h, \boldsymbol{\xi}_h^n + \theta \triangle \boldsymbol{\xi}_h, \triangle \boldsymbol{e}_h) : \triangle \boldsymbol{e}_h, \tag{26}$$

$$\triangle \boldsymbol{e}_h = \boldsymbol{e}(\triangle \boldsymbol{u}_h), \quad \triangle \boldsymbol{u}_h \in \boldsymbol{V}_h. \tag{27}$$

- Put $\boldsymbol{u}_h^{n+1} = \boldsymbol{u}_h^n + \triangle \boldsymbol{u}_h$, $\boldsymbol{\sigma}_h^{n+1} = \boldsymbol{\sigma}_h^n + \triangle \boldsymbol{\sigma}_h$, $\boldsymbol{\xi}_h^{n+1} = \boldsymbol{\xi}_h^n + \triangle \boldsymbol{\xi}_h$.

S3. **End**

The right hand side in (24) is determined through

$$(\triangle \boldsymbol{F}, \boldsymbol{v}_h) = \int_\Omega \triangle \boldsymbol{f}_{\mathrm{b}} \cdot \boldsymbol{v}_h \, \mathrm{d}\Omega + \int_{\Gamma_T} \triangle \boldsymbol{f}_{\mathrm{s}} \cdot \boldsymbol{v}_h \, \mathrm{d}\Gamma, \tag{28}$$

where

$$\triangle \boldsymbol{f}_{\mathrm{b}}(\boldsymbol{x}) = \boldsymbol{f}_{\mathrm{b}}(\boldsymbol{x}, t^{n+1}) - \boldsymbol{f}_{\mathrm{b}}(\boldsymbol{x}, t^n), \qquad \triangle \boldsymbol{f}_{\mathrm{s}}(\boldsymbol{x}) = \boldsymbol{f}_{\mathrm{s}}(\boldsymbol{x}, t^{n+1}) - \boldsymbol{f}_{\mathrm{s}}(\boldsymbol{x}, t^n).$$

Note that $\theta \in [0, 1]$ is a parameter. The choice of $\theta = 0$ resembles the forward (explicit) Euler method, $\theta = 1/2$ indicates the midpoint rule, and $\theta = 1$ corresponds to the backward (implicit) Euler scheme (see, e.g., [17]). Hence, the algorithm above refers to as the explicit ($\theta = 0$) and implicit ($\theta = 1$) incremental FE method, respectively. The question of consistency, numerical stability and accuracy of the forward and backward Euler integration algorithms is discussed in [22]. The essential difficulty in the incremental finite element method is the computation of $\boldsymbol{E}^{\mathrm{ep}}$ and $\boldsymbol{G}^{\mathrm{ep}}$ which depend at a fixed time step t^n on the stress and the vector of internal variables. Note that in the case $\theta = 0$ the values of $\partial \Phi / \partial \boldsymbol{\sigma}$, $\partial \Phi / \partial \boldsymbol{\xi}$, and $\boldsymbol{z}$ in (19) and (21) are computed at the beginning of the time increment and hence, at each time step they are known in advance.

Iterative solution schemes based on Newton's method to compute the increments $\triangle \boldsymbol{u}_h$, $\triangle \boldsymbol{\sigma}_h$, and $\triangle \boldsymbol{\xi}_h$ are widely used in the literature (cf., e.g., [4,5,19,22]). Typically, for each n, $0 \leq n \leq N$, in step S2 of the incremental FE algorithm, one has to solve a nonlinear system to find $\triangle \boldsymbol{u}_h$. The solution of this nonlinear system requires applications of Newton-like algorithms in which a sequence of linear problems has to be solved (see, e.g., [4]). The use of the so-called consistent tangent moduli within the finite element approach was first proposed in [19] where a consistently linearization of the nonlinear problem based on the closest-point return mapping algorithms is applied in order to preserve the quadratic

rate of asymptotic convergence of Newton's method. It was shown in the latter work that for associative J_2 plasticity with arbitrary rules of isotropic and kinematic hardening, an explicit expression for the tangent moduli consistent with the integration scheme can be derived. In the particular case of von Mises yield criterion with associative flow rule and isotropic hardening, the closest-point projection leads to the so-called radial return algorithm for which the consistent tangent matrix is easily computed (see [19] for details). A return mapping algorithm for the J_2 flow theory with isotropic hardening to compute the returned stress is presented in [17]. When the return is non-radial, an essential drawback in practical computations is the necessity of matrix inversions to solve the return equations (see, [17,2,22]).

4. Return mapping algorithm

We apply the return mapping algorithm based on the operator splitting methodology for the numerical solution of the elasto-plastic problem within the incremental FE method described in Section 3. For pioneering results in this area we refer the reader to [21] in case of simple plasticity models as, for instance, the linearly hardening von Mises plasticity with constant elastic moduli. The return mapping methods were further extended in [18] to elasto-plastic materials with non-associative plasticity, general yield conditions, arbitrary flow and hardening rules, and variable tangent elastic moduli. Details and generalizations of these algorithms can be found in [17].

For convenience of the presentation, we omit the discretization space parameter h and use the following notations for the increments: $\triangle\boldsymbol{\sigma} = \triangle\boldsymbol{\sigma}_h(\boldsymbol{x})$, $\triangle\boldsymbol{e} = \triangle\boldsymbol{e}_h(\boldsymbol{x})$, $\triangle\boldsymbol{\xi} = \triangle\boldsymbol{\xi}_h(\boldsymbol{x})$, at a fixed time step t^n, $0 \le n \le N$. For given initial values of $\boldsymbol{\sigma}^n$ and $\boldsymbol{\xi}^n$ the problem is to find the evolution of these values over the interval $[t^n, t^{n+1}]$.

The basic idea of the return algorithm is the following: A trial stress $\boldsymbol{\sigma}^{\text{trial}}$ is involved by taking the entire step to be elastic (elastic predictor). The computed trial stress is categorized to be elastic or plastic by checking the sign of the yield function Φ. If the predicted trial stress happens to fall outside the yield surface ($\Phi > 0$) then our assumption of elasticity has been wrong and the updated stress $\boldsymbol{\sigma}^{n+1}$ is obtained by the orthogonal projection (closest-point projection) of the trial stress onto the updated yield surface (plastic corrector). The return path is visualized in Fig. 1 in case of perfect plasticity (i.e., $\boldsymbol{\xi} \equiv \boldsymbol{0}$).

Using (2), (4), and (11) the final updated stress $\boldsymbol{\sigma}^{n+1}$ can be successively expressed as follows

$$\boldsymbol{\sigma}^{n+1} = \boldsymbol{E} : (\boldsymbol{e}^{n+1} - (\boldsymbol{e}^{\mathrm{p}})^{n+1}) \tag{29}$$

$$\boldsymbol{\sigma}^{n+1} = \boldsymbol{E} : (\boldsymbol{e}^{n+1} - (\boldsymbol{e}^{\mathrm{p}})^{n}) - \boldsymbol{E} : ((\boldsymbol{e}^{\mathrm{p}})^{n+1} - (\boldsymbol{e}^{\mathrm{p}})^{n}) \tag{30}$$

$$\boldsymbol{\sigma}^{n+1} = \boldsymbol{E} : \boldsymbol{e}^{n+1} - \boldsymbol{E} : \left(\boldsymbol{e}^{n} - (\boldsymbol{e}^{\mathrm{e}})^{n}\right) - \boldsymbol{E} : \triangle\boldsymbol{e}^{\mathrm{p}} \tag{31}$$

$$\boldsymbol{\sigma}^{n+1} = \boldsymbol{E} : (\boldsymbol{e}^{\mathrm{e}})^{n} + \boldsymbol{E} : (\boldsymbol{e}^{n+1} - \boldsymbol{e}^{n}) - \boldsymbol{E} : \triangle\boldsymbol{e}^{\mathrm{p}} \tag{32}$$

$$\boldsymbol{\sigma}^{n+1} = \boldsymbol{\sigma}^{n} + \boldsymbol{E} : \triangle\boldsymbol{e} - \triangle\gamma\, \boldsymbol{E} : \frac{\partial \Phi}{\partial \boldsymbol{\sigma}} \tag{33}$$

$$\boldsymbol{\sigma}^{n+1} = \boldsymbol{\sigma}^{\text{trial}} - \triangle\gamma\, \boldsymbol{E} : \frac{\partial \Phi}{\partial \boldsymbol{\sigma}}, \tag{34}$$

where $\triangle\gamma = \gamma^{n+1}\triangle t \ge 0$. This choice corresponds to the backward Euler scheme and leads to the classical return mapping algorithms (cf., [17]).

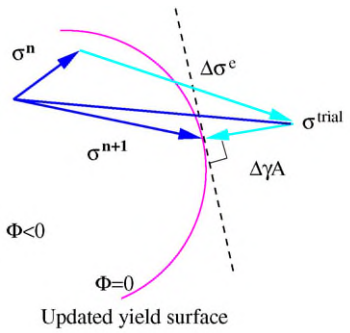

Fig. 1. Mapping the trial stress back to the yield surface (perfect plasticity)

For a given total strain increment $\triangle \boldsymbol{e}$ the following two steps are applied in the return mapping process:

1. *Elastic predictor*: Compute the trial stress $\boldsymbol{\sigma}^{\text{trial}}$ assuming only elastic behavior

$$\boldsymbol{\sigma}^{\text{trial}} = \boldsymbol{\sigma}^n + \triangle \boldsymbol{\sigma}^{\text{e}} \quad \text{with} \quad \triangle \boldsymbol{\sigma}^{\text{e}} = \boldsymbol{E} : \triangle \boldsymbol{e}. \tag{35}$$

2. *Plastic corrector*: Compute the updated stress and the internal variables

$$\boldsymbol{\sigma}^{n+1} = \boldsymbol{\sigma}^{\text{trial}} - \triangle \gamma \, \boldsymbol{A}, \quad \boldsymbol{A} = \boldsymbol{E} : \frac{\partial \Phi}{\partial \boldsymbol{\sigma}}, \tag{36}$$

$$\boldsymbol{\xi}^{n+1} = \boldsymbol{\xi}^n + \triangle \boldsymbol{\xi}, \quad \triangle \boldsymbol{\xi} = \triangle \gamma \, z, \tag{37}$$

where $\partial \Phi / \partial \boldsymbol{\sigma}$ and z are computed at the end of the time increment. Note that $\boldsymbol{A}$ is a second-order tensor called the projection direction (see Fig. 1). One can see from (33) that the updated stress $\boldsymbol{\sigma}^{n+1} = \boldsymbol{\sigma}^n + \triangle \boldsymbol{\sigma}$ can be evaluated with a stress increment $\triangle \boldsymbol{\sigma} = T(\boldsymbol{\sigma}^n, \boldsymbol{\xi}^n, \triangle \boldsymbol{e}) = T_n(\triangle \boldsymbol{e})$, computed by the return mapping procedure with a stress operator T_n determined according to the sign of the yield function Φ, namely

$$T_n(\triangle \boldsymbol{e}) = \begin{cases} \boldsymbol{E} : \triangle \boldsymbol{e}, & \text{if } \Phi(\boldsymbol{\sigma}^{\text{trial}}, \boldsymbol{\xi}^n) \leq 0, \\ \boldsymbol{E} : \triangle \boldsymbol{e} - \triangle \gamma \, \boldsymbol{E} : \dfrac{\partial \Phi}{\partial \boldsymbol{\sigma}}, & \text{if } \Phi(\boldsymbol{\sigma}^{\text{trial}}, \boldsymbol{\xi}^n) > 0. \end{cases} \tag{38}$$

Therefore, we simply set $\boldsymbol{\sigma}^{n+1} = \boldsymbol{\sigma}^{\text{trial}}$ in the case $\Phi(\boldsymbol{\sigma}^{\text{trial}}, \boldsymbol{\xi}^n) \leq 0$. Otherwise, one computes the plastic return of the trial stress onto the yield surface according to (36). The discrete plastic multiplier $\triangle \gamma$ is updated satisfying the yield condition at the end of the time increment

$$\Phi(\boldsymbol{\sigma}^{n+1}, \boldsymbol{\xi}^{n+1}) = 0. \tag{39}$$

In general, the return mapping of the trial stress back to the yield surface is nonlinear and it should be performed iteratively according to the Newton method with consistently linearized stress–strain relations. Thus, the proper choice of tangent moduli consistent with the proposed return mapping procedure has a strong influence on the convergence rate of the iterative schemes and the diminishing of the computational work. Consistent tangent moduli based on an exact linearization of the nonlinear problem have been originally proposed in [19] and recently developed, for instance, in [2].

In practical computations we emphasize on the classical von Mises constitutive relations which can be involved in various modifications (perfect plasticity or isotropic/kinematic hardening). We use as a model example the von Mises plasticity with isotropic strain hardening which fits to the porous composite ceramic materials when consider mechanical damages due to the growth and nucleation of voids. This model is given by

$$\Phi(\boldsymbol{\sigma}, \boldsymbol{\xi}) = \sqrt{\frac{3}{2}} \|\text{dev}(\boldsymbol{\sigma})\| - \mathcal{H}(\boldsymbol{\xi}) \tag{40}$$

$$\boldsymbol{\xi} = \sqrt{\frac{2}{3}} \|\boldsymbol{e}^{\text{p}}\|, \tag{41}$$

where $\text{dev}\,(\boldsymbol{\sigma}) = \boldsymbol{\sigma} - (1/3)\text{tr}(\boldsymbol{\sigma})\mathbf{1}$ denotes the deviatoric stress tensor and $\mathbf{1}$ is the second-order symmetric unit tensor. $\mathcal{H}$ is a given function derived experimentally. It is assumed to be twice differentiable with the following relations

$$\mathcal{H}(\boldsymbol{\xi}) \geq \mathcal{H}_0 > 0, \qquad \mathcal{H}'(\boldsymbol{\xi}) \geq \mathcal{H}_1 > 0, \qquad |\mathcal{H}''(\boldsymbol{\xi})| \leq \mathcal{H}_2, \quad \forall \boldsymbol{\xi} \geq 0. \tag{42}$$

The values of $\partial \Phi / \partial \boldsymbol{\sigma}$ and $\partial \Phi / \partial \boldsymbol{\xi}$ which take part in (19)and (21) can be easily computed

$$\frac{\partial \Phi}{\partial \boldsymbol{\sigma}} = \sqrt{\frac{3}{2}} \frac{\text{dev}(\boldsymbol{\sigma})}{\|\text{dev}(\boldsymbol{\sigma})\|}, \qquad \frac{\partial \Phi}{\partial \boldsymbol{\xi}} = -\mathcal{H}'. \tag{43}$$

The function $\mathcal{H}'(\boldsymbol{\xi})$ is called the isotropic hardening modulus. By (7), (11), and (41) we find z as follows

$$\dot{\boldsymbol{\xi}} = \sqrt{\frac{2}{3}} \|\dot{\boldsymbol{e}}^{\text{p}}\| = \sqrt{\frac{2}{3}} \gamma \left\| \frac{\partial \Phi}{\partial \boldsymbol{\sigma}} \right\| = \gamma z, \quad \Longrightarrow z = \sqrt{\frac{2}{3}} \left\| \frac{\partial \Phi}{\partial \boldsymbol{\sigma}} \right\| = 1. \tag{44}$$

Note that in this particular case the closest-point projection can be explicitly defined in such a way that no operator inversion is required. Here, one faces with the so-called radial return mapping algorithms whose efficiency is well established [17,19].

5. Structural optimization

The problem of structural optimization of microcellular biomorphic TiC-ceramics is discussed in this section. As noted in Section 1, the materials under consideration are microstructural and hence, their macroscopic mechanical behavior strongly depends on microscopic geometrical quantities such as the size of the voids and the lengths and widths of the different layers forming the cell walls (cf., e.g., [8]). While the size of the voids is determined by the growth of the wood itself (early/late wood), the other quantities can be influenced by tuning the parameters within the biotemplating process. For a given number of material layers m, we denote these geometrical quantities by $\boldsymbol{\alpha} = (\alpha_1, \ldots, \alpha_m)^{\mathrm{T}}$, further referred to as design parameters.

We consider a three-dimensional stationary microstructure with a geometrically simple tracheidal periodicity cell $Y = [0, 1]^3$ (see Fig. 2) consisting of an outer layer of carbon (C), interior layer of TiC, and a void channel (no material). In this particular case the number of layers is $m = 2$. We assume that our material workpiece occupies the bounded domain $\Omega \subset \mathcal{R}^3$ consisting of periodically distributed infinitesimal microstructures with three constituents (C, TiC, and Void).

The optimal structural design of the biomorphic microcellular ceramics can be performed by solving the structural optimization problem

$$J(\boldsymbol{u}, \boldsymbol{\alpha}) = \inf_{\boldsymbol{v}, \boldsymbol{\beta}} J(\boldsymbol{v}, \boldsymbol{\beta}), \tag{45}$$

subject to the following equality constraints.

The homogenized elasto-plastic equation of type (22) with $(\boldsymbol{E}^{\mathrm{ep}})^{\mathrm{H}}$ and $(\boldsymbol{G}^{\mathrm{ep}})^{\mathrm{H}}$,

$$\sum_{s=1}^{m} \alpha_s := C, \tag{46}$$

and the inequality constraints:

$$\alpha_s^{(\min)} \leq \alpha_s \leq \alpha_s^{(\max)}, \quad 1 \leq s \leq m, \tag{47}$$

where C is a given constant. The second equality in (46) and the bounds $\alpha_s^{(\min)}$, $\alpha_s^{(\max)}$, $1 \leq s \leq m$, in (47) stand for constraints motivated by both the microstructural geometry of the carbon preform and the biotemplating process. The von Mises plasticity with isotropic strain hardening is included in the homogenized elasto-plastic equation. The objective functional J depends on the mode of loading (cf., e.g., [8,16,3] for a variety of mechanical merit criteria).

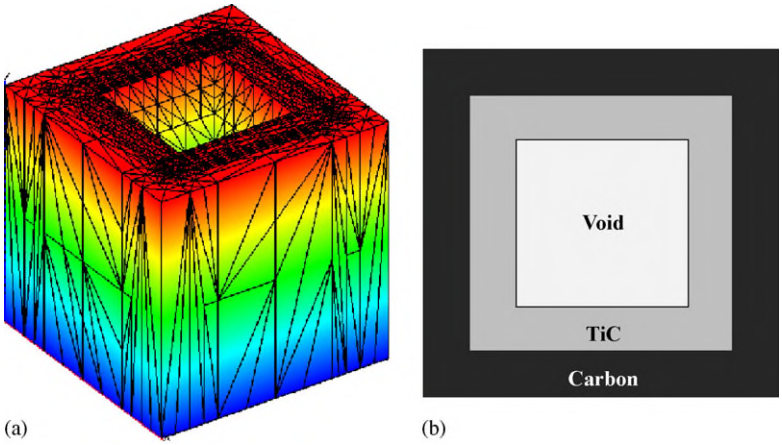

Fig. 2. (a) Periodicity cell $Y = [0, 1]^3$ and (b) cross section of $Y = \text{Void} \cup \text{TiC} \cup \text{C}$.

Note that the resolution of the microstructures is cost prohibitive with respect to computational work. Thus, the main idea is to derive a homogenized macromodel featuring the dependence on the microstructural design variables and to apply the optimization process to the homogenized macrostructure. Typically, the microscopic and macroscopic models are considered simultaneously supposing a strong scale separation, i.e., a large gap in length scale between the macroscopic component and the microstructure. A double-scale asymptotic expansion for the displacement rate and a homogenization procedure by taking a zero limit of the scale ratio are applied to come up with computationally feasible macromodel. For layered materials the fourth-order tensor $(\boldsymbol{E}^{\mathrm{ep}})^{\mathrm{H}} = (\boldsymbol{E}^{\mathrm{ep}})^{\mathrm{H}}(\boldsymbol{\alpha})$ (also called homogenized elasto-plastic tangent modulus) and $(\boldsymbol{G}^{\mathrm{ep}})^{\mathrm{H}} = (\boldsymbol{G}^{\mathrm{ep}})^{\mathrm{H}}(\boldsymbol{\alpha})$ in (46) corresponding to the homogenized model can be explicitly obtained taking into account the expressions $\boldsymbol{E}_s^{\mathrm{ep}}$ and $\boldsymbol{G}_s^{\mathrm{ep}}$ of all material layers, $1 \le s \le m$. Note that in this case $\boldsymbol{E}_s^{\mathrm{ep}} = \boldsymbol{E}_s$ and $\boldsymbol{G}_s^{\mathrm{ep}} = \boldsymbol{0}$ if the sth layer is elastic (see, e.g., [13], Chapter 5).

In our model the computation of the averaged stresses and strains from the constitutive relations has to be done numerically. Effective elasto-plasticity properties of periodic microstructural composite materials based on the homogenization approach are considered in [7,14,20]. The following expression for the homogenized elasto-plastic tangent modulus holds (see, e.g., [7])

$$(E_{ijk\ell}^{\mathrm{ep}})^{\mathrm{H}} = \frac{1}{|Y|}\int_Y E_{ijqr}^{\mathrm{ep}}\left(I_{qr}^{kl} + \frac{\partial \zeta_q^{k\ell}}{\partial y_r}\right)\mathrm{d}Y, \tag{48}$$

where E_{ijqr}^{ep} are the components of the instantaneous tangent modulus and I_{qr}^{kl} is the fourth-order identity tensor given by

$$I_{qr}^{kl} = \frac{1}{2}(\delta_{qk}\delta_{rl} + \delta_{ql}\delta_{rk}).$$

The third-order tensor $\boldsymbol{\zeta} = (\zeta_q^{k\ell})$ has Y-periodic (i.e., equal values on opposite sides of Y) entries $\zeta_q^{k\ell} \in H^1(Y)$ referred to as characteristic displacements. Note that $\boldsymbol{\zeta}^{k\ell}$ are computed by solving the elasto-plasticity problem in the unit cell Y with periodic boundary conditions. The Young modulus E (in GPa) and the Poisson ratio ν of our two materials are, respectively, $E = 10$, $\nu = 0.22$ for carbon and $E = 439$, $\nu = 0.187$ for TiC. In case of elastic behavior of the composite material numerous computational results are given in [9] for a two-dimensional specimen and in [11] for a three-dimensional material workpiece.

To find the homogenized coefficients (48) we use finite element discretizations of the computational domain Y. The periodic microcell is decomposed first in hexahedra and further by continuous, piecewise linear finite elements on tetrahedral shape regular meshes, as shown in Fig. 3. Recently, we have developed adaptive grid refinement algorithms using the Zienkiewicz–Zhu a posteriori error estimator originally proposed in [23] for elasticity problems. Based on an averaging technique we find the nodal values of the recovered stress $\boldsymbol{\sigma}^*$ and the discrete stress $\hat{\boldsymbol{\sigma}}$ locally and compute the error indicator for each tetrahedral finite element T as follows

$$\eta_T := \|\boldsymbol{\sigma}^* - \hat{\boldsymbol{\sigma}}\|_{0,T}. \tag{49}$$

Furthermore, we mark for refinement those tetrahedra $\{T\}$ for which

$$\eta_T \ge \beta \max_{T'} \eta_{T'},$$

where $0 < \beta < 1$ is a prescribed threshold, for instance, $\beta = 0.5$. Note that the adaptive mesh-refinement procedure is local and computationally cheap. Details are given in [9]. Efficient solvers for the linear systems in the three-dimensional elastic model are discussed in [11]. Some numerical experiments from the computation of the homogenized elasticity coefficients with respect to the consecutive number of adaptive level are presented in Tables 1 and 2.

Our implementation of the incremental finite element method is based on adaptivity in the space discretization by using a posteriori error estimators. The adaptive grid refinement within the computation of (24) and (25) in step S2 of the algorithm requires additionally to define and compute the error indicator, to refine the mesh, to generate a new finite element space, and to transfer the evaluated data from the previous time step according to the new discretization. Hence, during a fixed time increment the finite element discretization of the domain is updated and one has to take care of sufficiently accurate approximate solutions. Our adaptivity procedure in the elasto-plasticity model relies on the Zienkiewicz–Zhu type error indicator considering the error energy norm based on the corresponding elasticity operator.

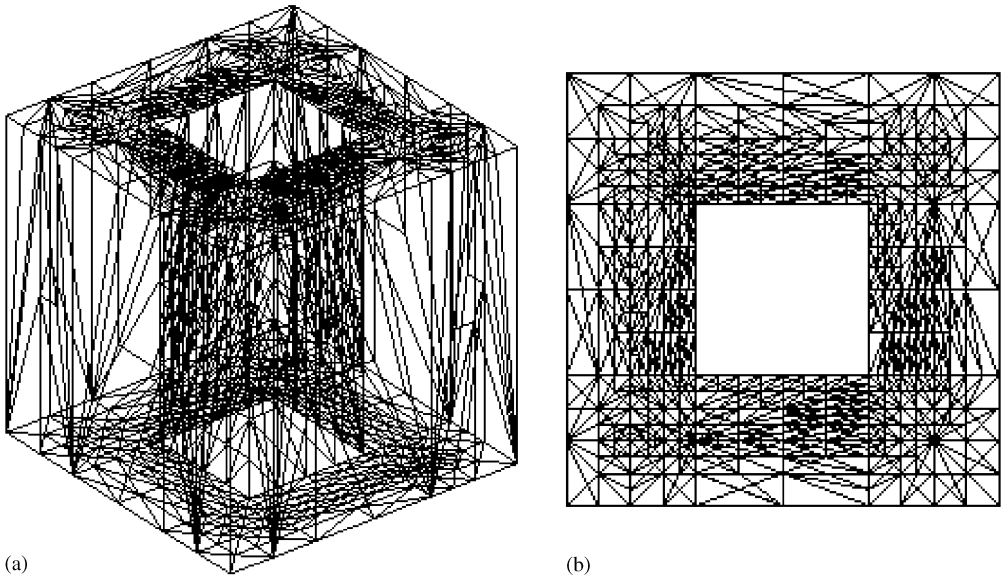

(a) (b)

Fig. 3. Adaptive refinement: (a) 3D unit periodicity cell Y and (b) cross section of Y.

Table 1
Homogenized coefficients w.r.t. the adaptive refinement level, density 19%

Level	E^{H}_{1111}	E^{H}_{2222}	E^{H}_{3333}	E^{H}_{1212}	E^{H}_{2323}	E^{H}_{1313}
1	179.7	192.4	224.2	67.4	75.5	64.0
2	197.4	227.0	238.1	80.7	99.1	69.8
3	177.6	188.7	226.9	60.9	73.1	63.1
4	190.2	184.3	235.7	69.7	72.0	81.5
5	184.5	180.6	236.1	46.3	57.4	86.6
6	171.5	156.0	228.1	31.0	58.3	56.9
7	177.6	151.5	234.1	29.1	59.1	76.8
8	170.9	152.7	232.5	26.5	59.3	64.4
9	161.6	148.9	230.0	36.6	57.8	59.2
10	146.9	145.7	230.3	28.5	55.2	57.3

The stress computation procedure plays an essential role in the efficiency of the incremental finite element method. We use the return mapping stress operator (38) defined in the previous section. Numerically the most consuming part of the incremental algorithm is the solution of the nonlinear system (24) and (25) which has to be done at each time step n, $0 \leq n \leq N$. For simplicity, using an isomorphism $\mathcal{R}^{M_n} \to \boldsymbol{V}_{h_n}$, we write this system in the following algebraic

Table 2
Homogenized coefficients w.r.t. the adaptive refinement level, density 84%

Level	E^{H}_{1111}	E^{H}_{2222}	E^{H}_{3333}	E^{H}_{1212}	E^{H}_{2323}	E^{H}_{1313}
1	168.6	174.2	180.2	63.6	66.8	62.3
2	178.6	191.1	194.7	75.2	79.7	71.4
3	167.2	179.1	192.3	63.9	70.7	68.8
4	172.7	157.3	188.9	51.4	60.2	70.8
5	154.0	153.1	192.0	48.1	63.1	64.0
6	123.5	125.4	190.0	37.9	51.1	51.0
7	104.7	109.8	187.9	34.4	46.8	50.3
8	99.6	99.7	187.7	30.4	48.1	48.4
9	88.1	90.3	186.3	26.5	45.0	46.2
10	84.0	84.3	185.8	26.6	43.8	43.5

form

$$\mathcal{F}_n(\triangle \boldsymbol{u}) = \triangle \boldsymbol{f}^n, \quad \triangle \boldsymbol{u}, \triangle \boldsymbol{f}^n \in R^{M_n}, \tag{50}$$

where M_n is the number of degrees of freedom for the finite element mesh and h_n is the discretization parameter at the nth time step. The nonlinear operator $\mathcal{F}_n : \mathcal{R}^{M_n} \to \mathcal{R}^{M_n}$ is defined by

$$< \mathcal{F}_n(\boldsymbol{u}), \boldsymbol{v} >= \int_Y T_n(\boldsymbol{e}(\boldsymbol{u}_h)) : \boldsymbol{e}(\boldsymbol{v}_h)\, \mathrm{d}Y, \quad \forall \boldsymbol{u}, \boldsymbol{v} \in \mathcal{R}^{M_n}, \tag{51}$$

where $< \boldsymbol{u}, \boldsymbol{v} >= \boldsymbol{u} \cdot \boldsymbol{v}$ and $\boldsymbol{u}_h, \boldsymbol{v}_h$ are the finite element functions corresponding to $\boldsymbol{u}, \boldsymbol{v}$.

The system (50) can be solved iteratively by Newton-like method of the form

$$\triangle \boldsymbol{u}^i = \text{given} \tag{52}$$

$$\boldsymbol{r}^{n,i} = \triangle \boldsymbol{f}^n - \mathcal{F}_n(\triangle \boldsymbol{u}^i) \tag{53}$$

$$A_{n,i}\boldsymbol{\delta}^i = \boldsymbol{r}^{n,i} \tag{54}$$

$$\triangle \boldsymbol{u}^{i+1} = \triangle \boldsymbol{u}^i + \omega_i \boldsymbol{\delta}^i, \tag{55}$$

where $\omega_i \in (0, 1]$ is a damping parameter. The initial guess $\triangle \boldsymbol{u}^0$ can be zero or the computed value of $\triangle \boldsymbol{u}$ from the previous time step. The choice of the matrix $A_{n,i}$ in the linear system (54) and the efficient linear solver have a strong influence on the accuracy of the numerical solution. A standard technique is to use the so-called initial stiffness method for which $A_{n,i}$ is the stiffness matrix corresponding to the elasticity operator. If the Frechet derivative $\mathcal{F}'_n$ of the nonlinear operator in (50) exists, one can consider the Newton method with $A_{n,i} = \mathcal{F}'_n(\triangle \boldsymbol{u}^i)$. Inexact (i.e., solving (54) iteratively) Newton-like solvers are computationally cheaper than direct methods especially for large-scale elasto-plasticity. Convergence of inexact Newton solvers and basic properties of $\mathcal{F}_n$ for return mapping stress computations are studied in [5]. A proper combination of the inexact initial stiffness method and the inexact Newton method is proposed in [4].

Our numerical experiments concern the incremental return mapping algorithm with inexact initial stiffness method, i.e., $A_{n,i}$ corresponds to the elasticity stiffness matrix which is symmetric and positive definite but not an M—matrix. We apply the preconditioned conjugate gradient (PCG) method for solving the auxiliary linear system (54) with two types of preconditioners: Incomplete Cholesky (IC) factorization and Algebraic MultiGrid (AMG) preconditioner. The nonlinear system (50) is solved iteratively at each time step with a number of iterations determined by the following stopping criterion

$$\|\boldsymbol{r}^{n,i}\| \leq \varepsilon \|\triangle \boldsymbol{f}^n\|,$$

where ε is a given tolerance, for instance, $\varepsilon = 10^{-4}$. For solving the auxiliary linear system to find the correction $\boldsymbol{\delta}^i$ we use a relative condition for the residual norm of the form

$$\|A_{n,i}\boldsymbol{\delta}^i - \boldsymbol{r}^{n,i}\| \leq \eta \|\boldsymbol{r}^{n,i}\|,$$

where η is a given accuracy parameter, taken in the experiments as $\eta = 10^{-2}$.

In Table 3 we report some computational results for finding the characteristic displacement $\boldsymbol{\zeta}^{11}$ in the unit microcell with various density of the solid material part. We consider a time discretization with a step size $\triangle t = 1/10\,(N = 9)$ and report the number of degrees of freedom M_N at the last adaptive refinement level. We denote by TNNLI the total number of nonlinear iterations and by TNLI the total number of linear iterations using PCG as a computational solver. One can observe from the numerical experiments a better convergence with respect to the number of iterations for the AMG method compared to IC preconditioner. Various other preconditioners can be tested to get more efficient linear solvers. One expects a faster convergence using the inexact Newton method for solving the nonlinear system.

The dependence of the homogenized elasto-plastic tangent modulus $(\boldsymbol{E}^{\mathrm{ep}})^{\mathrm{H}} = (\boldsymbol{E}^{\mathrm{ep}})^{\mathrm{H}}(\boldsymbol{\alpha})$ on the design parameters $\boldsymbol{\alpha}$ is found by means of multivariate interpolation. Primal-dual Newton interior point methods for solving the structural optimization problem with a suitable steplength selection and various strategies for convergence monitoring are discussed in [10].

Table 3
Convergence results: $N = 9$, $\varepsilon = 10^{-4}$, $\eta = 10^{-2}$

Density (%)	M_N	TNNLI	TNLI (IC)	TNLI (AMG)
19	13336	17	876	293
51	16066	20	928	312
75	18430	23	943	325
84	19492	25	996	341

6. Conclusions

Structural optimization of biomorphic ceramic composites is considered. The new materials are produced using a naturally grown wood by a two-steps processing: high-temperature pyrolysis of the wooden specimen and infiltration reaction of the carbonized wood with various carbide forming metals (e.g., Si, Ti). Homogenization approach is applied to obtain the macromodel with a cubic microstructure of three phases (carbon, carbide material, and a void) supposed to be periodically distributed throughout the design media. The lengths and widths of the different material layers forming the cell walls are considered as design parameters. These variables can be tuned very precisely during the processing and have a significant impact on the macroscopic mechanical behavior of the final ceramics.

The homogenized elasto-plastic equation is invoked as an equality constraint in the structural optimization problem. Additionally, we have inequality constraints motivated by the microstructural geometry. The incremental finite element method is used for the numerical solution of the elasto-plastic problem. Newton-like iterative algorithms are applied to solve the nonlinear system of equations during the time increments. A return mapping scheme is considered for the stress computation procedure defined as a closest-point projection of the trial elastic stress onto the yield surface. The latter method was extensively developed in the last decade and has become a popular tool in computational plasticity due to its efficiency, accuracy, and stability.

Tetrahedral shape regular decomposition and adaptive grid refinement techniques based on a posteriori error estimators are used for the finite element discretization of the microstructure. Numerical experiments for the computation of the homogenized elasticity coefficients are presented for microcells of small/large density. Convergence results with respect to the total number of nonlinear and linear iterations using various efficient linear iterative solvers are compared and discussed.

Acknowledgments

This work has been partially supported by the German National Science Foundation (DFG) under Grant HO877/5-3. The first author has also been supported by the NSF under Grant No. DSM-0411403. The research of the second author has been sponsored in part by Grant I1402/2004 of the Bulgarian Ministry for Education and Science.

References

[1] G. Allaire, Shape Optimization by the Homogenization Method, Springer, New York, 2002.
[2] G. Asensio, C. Moreno, Linearization and return mapping algorithms for elastoplasticity models, Int. J. Numer. Methods Eng. 57 (2003) 991–1014.
[3] M.F. Ashby, Materials and shape, Acta Metall. 39 (1991) 1025–1039.
[4] O. Axelsson, R. Blaheta, R. Kohut, Inexact Newton solvers in plasticity: theory and experiments, Numer. Lin. Algebra Appl. 4 (3) (1997) 133–152.
[5] R. Blaheta, Convergence of Newton-type methods in incremental return mapping analysis of elasto-plastic problems, Comput. Methods Appl. Mech. Eng. 147 (1997) 167–185.
[6] M.C. Delfour, J.-P. Zolésio, Shapes and Geometries. Analysis, Differential Calculus, and Optimization, SIAM, Philadelphia, 2001.
[7] S. Ghosh, K. Lee, S. Moorthy, Two scale analysis of heterogeneous elastic–plastic materials with asymptotic homogenization and Voronoi cell finite element model, Comput. Methods Appl. Mech. Eng. 132 (1–2) (1996) 63–116.
[8] L.J. Gibson, M.F. Ashby, Cellular Solids, Structure, and Properties, Pergamon Press, New York, 1988.
[9] R.H.W. Hoppe, S.I. Petrova, Optimal shape design in biomimetics based on homogenization and adaptivity, Math. Comput. Simul. 65 (3) (2004) 257–272.
[10] R.H.W. Hoppe, S.I. Petrova, Primal-dual Newton interior point methods in shape and topology optimization, Numer. Lin. Algebra Appl. 11 (5–6) (2004) 413–429.

[11] R.H.W. Hoppe, S.I. Petrova, Efficient solvers for 3-D homogenized elasticity model, in: J. Dongarra et al. (Eds.), Lecture Notes Comput. Sci., vol. 3732, Springer, 2006, pp. 857–863 (http://www.informatik.uni-trier.de/~ley/db/conf/para/para2004.html#HoppeP04).
[12] V.V. Jikov, S.M. Kozlov, O.A. Oleinik, Homogenization of Differential Operators and Integral Functionals, Springer, 1994.
[13] P.B. Lourenco, Computational strategies for masonry structures, Ph.D. Thesis, Delft University of Technology, The Netherlands, 1996.
[14] J.C. Michel, H. Moulinec, P. Suquet, Effective properties of composite materials with periodic microstructure: a computational approach, Comput. Methods Appl. Mech. Eng. 172 (1999) 109–143.
[15] T. Ota, M. Takahashi, T. Hibi, M. Ozawa, S. Suzuki, Y. Hikichi, H. Suzuki, Biomimetic process for producing SiC wood, J. Am. Ceram. Soc. 78 (1995) 3409–3411.
[16] G.I.N. Rozvany, Structural Design via Optimality Criteria. The Prager Approach to Structural Optimization, Kluwer, Dordrecht, 1989.
[17] J.C. Simo, T.J.R. Hughes, Computational Inelasticity, Springer, 1998.
[18] J.C. Simo, M. Ortiz, A unified approach to finite deformation elastoplastic analysis based on the use of hyperelastic constitutive equations, Comput. Methods Appl. Mech. Eng. 49 (1985) 221–245.
[19] J.C. Simo, R.L. Taylor, Consistent tangent operators for rate-independent elastoplasticity, Comput. Methods Appl. Mech. Eng. 48 (1985) 101–118.
[20] C.C. Swan, A.S. Cakmak, Homogenization and effective elastoplasticity models for periodic composites, Commun. Numer. Methods Eng. 10 (1994) 257–265.
[21] M.L. Wilkins, Calculation of Elasto-plastic Flow, Methods of Computational Physics, vol. 3, Academic Press, New York, 1964.
[22] Z.L. Zhang, Explicit consistent tangent moduli with a return mapping algorithm for pressure-dependent elastoplasticity models, Comput. Methods Appl. Mech. Eng. 121 (1995) 29–44.
[23] O.C. Zienkiewicz, J.Z. Zhu, A simple error estimator and adaptive procedure for practical engineering analysis, Int. J. Numer. Methods Eng. 24 (1987) 337–357.